PNAS
www.pnas.org

Supplementary Information for

Magnetic handshake materials: a new platform for scale invariant programmed self-assembly

Ran Niu[a,*], Chrisy Xiyu Du[b], Edward Esposito[a], Jakin Ng[a], Michael Brenner[b], Paul McEuen[a,c] & Itai Cohen[a,c,*1]

[a]Laboratory of Atomic and Solid State Physics, Cornell University, Ithaca, New York, 14853, USA; [b]School of Engineering and Applied Sciences, Harvard University, Cambridge MA 02139, USA; [c]Kavli Institute at Cornell for Nanoscale Science, Cornell University, Ithaca, New York, 14853, USA

E-mail: rn362@cornell.edu or ic64@cornell.edu

This PDF file includes:

Supplementary text
Figs. S1 to S8
Captions for Movies S1 to S7

Other supplementary materials for this manuscript include the following:

Movies S1 to S7

www.pnas.org/cgi/doi/10.1073/pnas.1910332116

Supporting Information Text

Theoretical Model

Interaction between pairs of $N \times N$ Panels. In our theoretical model, we assume each magnet acts as a perfect magnetic dipole. Thus the potential (V) and force (F) between two magnets can be expressed as

$$V(\vec{r}) = -\frac{\mu_0}{4\pi|\vec{r}|^3}\left[3(\vec{m}_1\cdot\hat{r})(\vec{m}_2\cdot\hat{r}) - \vec{m}_1\cdot\vec{m}_2\right] \quad [1]$$

$$\vec{F}(\vec{r}) = \frac{3\mu_0}{4\pi|\vec{r}|^4}\Big[(\hat{r}\times\vec{m}_1)\times\vec{m}_2 + (\hat{r}\times\vec{m}_2)\times\vec{m}_1 - 2\hat{r}(\vec{m}_1\cdot\vec{m}_2) + 5\hat{r}\big((\hat{r}\times\vec{m}_1)\cdot(\hat{r}\times\vec{m}_2)\big)\Big], \quad [2]$$

where μ_0 is the vacuum permeability, $\vec{m}_1$ is the magnetic moment for magnet 1, $\vec{m}_2$ is the magnetic moment for magnet 2, and $\vec{r}$ is the separation between the two magnets.

In the case where $|m_1| = |m_2| = m$ and $\vec{m}_1, \vec{m}_2, \vec{r}$ are all in the same direction, we can simplify the equation to

$$\vec{F}(\vec{r}) = \frac{3\mu_0}{4\pi r^4}[-2\hat{r}(\vec{m}_1\cdot\vec{m}_2)] = -\frac{3\mu_0 m^2}{2\pi r^4}\hat{r} \quad [3]$$

$$V(r) = -\frac{\mu_0 m^2}{2\pi r^3} \quad [4]$$

The magnetic moment can be written as $m = B_r\mathrm{Vol}/\mu_0$, where B_r is the residual flux density, and Vol is the volume of the magnet. Since B_r is a material dependent quantity, for the same materials, the binding energy between two magnetic dipoles scales with the volume of the magnet.

The cumulative potential (force) between two panels of $N \times N$ arrays of dipole patterns can be expressed as a sum of all potentials (forces) between any pair of magnets that do not belong to the same panel, which is

$$V_{\text{panel}} = \sum_{i,j} V(\vec{r_{ij}}) \qquad \text{(Dipole i and j do not belong to the same magnetic panel)} \quad [5]$$

$$F_{\text{panel}} = \sum_{i,j} F(\vec{r_{ij}}) \quad [6]$$

When calculating the cumulative potential (force) between two panels using Eq. 5, 6, there are two competing length scales. One of the length scale is the separation d between the center of mass of the two panels, and the other length scale is the lateral separation a between the two adjacent magnets in the same panel. The separation d governs the nearest neighbor interaction strength and a plays an important role when thinking about second nearest neighbor or third nearest neighbor interactions. Using a, d and the amplitude of magnetic dipole moment m, we can write down the functional form of the potential (force) for all four panels.

Potentials of the four panels:

$$\text{Black Panel: } V = -\frac{2\mu_0 m^2}{\pi}\left[\frac{1}{d^3} + \frac{2d^2-a^2}{(a^2+d^2)^{5/2}} + \frac{d^2-a^2}{(2a^2+d^2)^{5/2}}\right] \quad [7]$$

$$\text{Green Panel: } V = -\frac{2\mu_0 m^2}{\pi}\left[\frac{1}{d^3}\right] \quad [8]$$

$$\text{Blue Panel: } V = -\frac{2\mu_0 m^2}{\pi}\left[\frac{1}{d^3} + \frac{a^2-d^2}{(2a^2+d^2)^{5/2}}\right] \quad [9]$$

$$\text{Red Panel: } V = -\frac{2\mu_0 m^2}{\pi}\left[\frac{1}{d^3} + \frac{a^2-2d^2}{(a^2+d^2)^{5/2}} + \frac{d^2-a^2}{(2a^2+d^2)^{5/2}}\right] \quad [10]$$

Forces of the four panels:

$$\text{Black Panel: } F = \frac{3\mu_0 m^2 d}{\pi}\left[\frac{2}{d^5} + \frac{4d^2-6a^2}{(a^2+d^2)^{7/2}} + \frac{2d^2-6a^2}{(2a^2+d^2)^{7/2}}\right] \quad [11]$$

$$\text{Green Panel: } F = \frac{3\mu_0 m^2 d}{\pi}\left[\frac{2}{d^5}\right] \quad [12]$$

$$\text{Blue Panel: } F = \frac{3\mu_0 m^2 d}{\pi}\left[\frac{2}{d^5} + \frac{6a^2-2d^2}{(2a^2+d^2)^{7/2}}\right] \quad [13]$$

$$\text{Red Panel: } F = \frac{3\mu_0 m^2 d}{\pi}\left[\frac{2}{d^5} + \frac{6a^2-4d^2}{(a^2+d^2)^{7/2}} + \frac{2d^2-6a^2}{(2a^2+d^2)^{7/2}}\right] \quad [14]$$

For the potential (force) of the panels, they all have the same prefactor, which is determined by the magnetic moment m. This shows that the strength of panel binding energies also scales with the magnet volume. However, the relative binding energy difference between the four panels solely depends on the relationship between a and d. By controlling the closest contact distance between two panels, we can also modulate the binding energy level within the four different panels. In experiments, we can control this distance by adding or removing spacers. Since the binding energy of the four panels decays differently as a function of separation, as we increase the ratio between d and a, the binding energy separation will also increase. For example, when $d = a$, $V_{\text{Black}} : V_{\text{Green}} : V_{\text{Blue}} : V_{\text{Red}} = (1 + 2^{-5/2}) : 1 : 1 : (1 - 2^{-5/2}) \approx 1.177 : 1 : 1 : 0.823$, while when $d = 2a$, $V_{\text{Black}} : V_{\text{Green}} : V_{\text{Blue}} : V_{\text{Red}} = (1 + 56\sqrt{5}/125 + \sqrt{6}/9) : 1 : (1 - \sqrt{6}/9) : (1 - 56\sqrt{5}/125 + \sqrt{6}/9) \approx 2.274 : 1 : 0.728 : 0.270$. The relative scale of the binding energies will hold in any length scale as long as the ratio between a and d is fixed.

We also verified this theoretical model with experimental measurements by comparing the magnetic forces measured in the perpendicular direction of the four unique panels to the forces from theoretical calculation. In experiments, $d = 0.65$cm and $a = 0.3$cm, so in our calculation, we will set $d = 2a$. Upon scaling the distance and binding force to match the experimental units, the theoretical calculations agree quantitatively with experimental results (Fig. 1B in main text).

Additionally, we computed the binding energy between any two pair of the four panels. Since we do not know *a priori* the configuration between non-optimal pairing panels that minimizes the binding energy, we performed gradient descent to find the optimal relative position and orientation between the two panels (Fig. 1E in main text). The code is available upon request.

Magnetic Strands. To calculate the debinding behavior of magnetic strands from a pairing configuration analytically, we need to enumerate all the possible states of the two magnetic strands and calculate the probability of binding with increasing temperature. To simplify the calculation of the partition function, we make the following assumptions based on experimental conditions:

1. The system is in 2D and the strands can only rotate along the axis perpendicular to the 2D plane.
2. There is no unfavorable binding.
3. There is no vibration when two panels bind.
4. There is no partial binding.
5. We treat the strands as rigid bodies.

With these assumptions, we can calculate the partition function $\sum_\Omega Q_\Omega$ of two strands with N binding sites at various temperatures. For each state Ω, there are three parts contributing to the partition function:

$$Q_\Omega = q_t^{(\Omega)} q_r^{(\Omega)} e^{-E_\Omega / k_B T}, \tag{15}$$

where q_t is the translational degree of freedom, q_r is the rotational degree of freedom, and E_Ω is the energy contribution. Since the system is two dimensional, $q_t \sim (Nmk_BT)$. As we assume one degree of freedom for rotation, $q_r \sim (k_BT)^{1/2}(mN^3l^2/12)^{1/2}$. Here N is the number of binding sites, and l is the distance between two binding sites. The resulting q_r is based on the moment of inertia tensor of a cylinder.

With these settings, the partition function contribution of two free strands is

$$q_{\text{free}} = (q_{\text{single}})^2 \sim [(Nmk_BT)(k_BT)^{1/2}(mN^3l^2/12)^{1/2}]^2 \tag{16}$$

The partition function contribution of two completely bound strands is

$$q_{\text{bond}} \sim (N2mk_BT)(k_BT)^{1/2}(2mN^3l^2/12)^{1/2} \exp(-\sum_{k=1}^{N} E_k/k_BT) \tag{17}$$

Since we assume that there is no partial binding, the partition function is just

$$\mathcal{Z} = q_{\text{free}} + q_{\text{bond}}, \tag{18}$$

and the binding probability of two strands is $q_{\text{bond}}/\mathcal{Z}$. Now we can calculate the binding probability of pairing strands as a function of temperature. Fig.3A i-iv in the main text show the calculated results of four different scenarios matching the experimental results. Note that in experiments, there is no temperature but rather the acceleration Γ from the shaker, so the mapping between temperature in the theoretical framework and the acceleration in the experiments is non-trivial. Thus we apply a consistent arbitrary scaling parameter to match the theoretical calculation to the experimental data. All the analytically calculated curves agree qualitatively with the experimental data and most of them have similar slopes. We do observe broader melting curves for the calculations, especially in the low probability region at higher Γ. Such deviations are expected, since the experiment consists of measurements on a small number of paired strands. For such finite system sizes one expects a systematic deviation from theoretical calculations especially in regions of low probability. Such rare states can be missed for small system sizes. Additionally, the experimental system is not strictly thermal. Nevertheless, these calculations do provide some intuition as is evidenced by the fact that their shape does depend on our detailed accounting of the entropy and the fact that despite their limitations they fit the experimental data rather well.

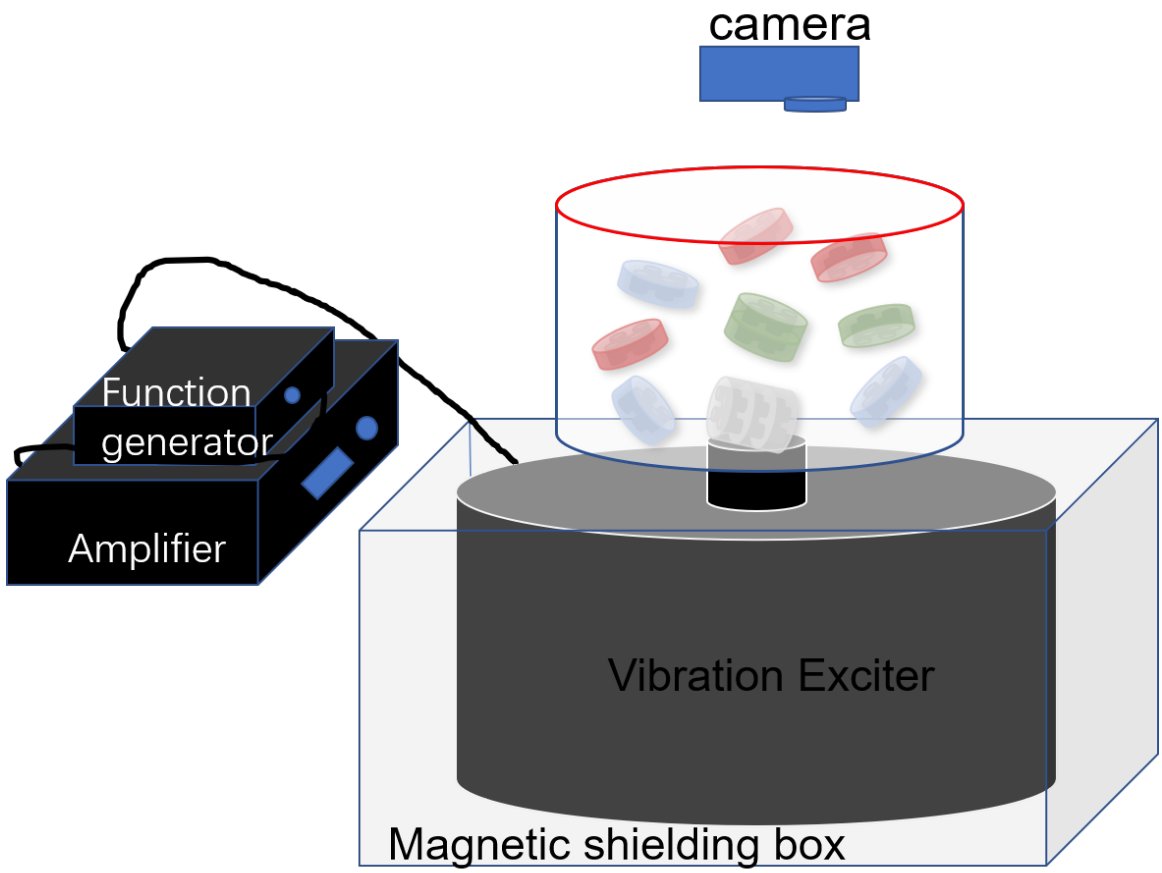

Fig. S1. Shaker Table: We designed an experimental setup made of a vibration shaker controlled by an amplifier and a function generator, a magnetic shielding box blocking the magnetic field from the shaker, a sample cell of tunable height and a camera for video recording.

Experimental Methods

Shaker Table. The vertical vibration is generated by a vertical vibrator (Type4808, Brüel & Kjær North America, Inc.) driven by a function generator (3011B, BK PRECISION®) and an amplifier (Type2719, Brüel & Kjær North America, Inc.). To prevent the permanent magnets in the shaker from influencing the self-assembly of our magnetic building blocks, we made a thick, low carbon steel box (Amuneal, USA) to shield the magnetic field from the permanent magnet. We designed a sample cell of tunable height and screwed it to the vibrational shaker head. After shielding, the magnetic field in the sample cell is equal to earth's magnetic field as measured by a Gaussmeter.

The vertical displacement function is $A\sin(2\pi ft)$, where A and f are the amplitude and frequency of vibration, respectively. The acceleration $\Gamma = 4\pi^2 f^2 A$ (in units of g) was directly measured by a portable accelerometer (ADXL345, Sparkfun Electronics) mounted vertically on the outer edge of the sample cell. During the experiments, we fix the frequency f at 25Hz and tune Γ by the vibration amplitude. The self-assembly of panels, strands and 2D nets was recorded with a high-speed camera (GoPro) from the top at a frame rate of 120Hz.

Acceleration and force. The panels need to be agitated at a large enough Γ for bond breaking. In particular, Γ needs to be larger than g to get the structures bouncing and practically significantly larger than g for bond breaking. However, the energy from shaking a structure is distributed and can be focused to create large forces. In our case even the three-body interaction of the two panels and the shaker can in some rare configurations cause large forces at relatively low Γ (still high enough to overcome g but well below the transition Γ). This effect can be seen from experiments where we load two panels into the shaker and determine the binding statistics as a function of Γ. We find that the transition is not perfectly sharp (Fig. S2).

Acceleration and effective temperature. The shaker agitation provides an energy scale to the panels and strands. We can draw a loose connection between the shaker strength and an effective temperature by writing down the equation of motion of the ith panel following the Langevin equation:

$$m_i \frac{d^2\vec{r_i}}{dt^2} = -\lambda \frac{d\vec{r_i}}{dt} - \nabla V(\vec{r_i}) + \vec{\eta}(t).$$

Here, m_i is the panel mass, $\vec{r_i}$ is the position of the panel and λ is the effective damping force. $V(\vec{r_i})$ is the magnetic potential felt by the panel and η is the noise term that is generated by the shaker. In a thermal system, the damping force can be related to a viscosity and the noise term can be related to an effective temperature via $\langle \eta^2(t) \rangle = 2\lambda k_{\mathrm{B}} T_{\mathrm{eff}}$. In our macroscale system, such relationships are more complicated. For example, we can measure the velocity distribution of panels at different shaking strength and loosely map the shaking strength Γ to an effective temperature by looking at the most probable velocity $v_p \sim \sqrt{k_{\mathrm{B}} T_{\mathrm{eff}}/m}$. This latter interpretation has a rich history in the field of granular matter and has some obvious caveats. For example, the energy is being injected at one frequency scale, and it is not *a priori* clear how this energy cascades to excitation modes with different frequencies. As another example, energy focusing from torque inducing collisions with the shaker surface can play an important role in breaking the bonds of our assemblies. Still, there are features of our macroscale system that sufficiently resemble microscale thermal systems that make this interpretation useful for building intuition. For example, Fig. S3 shows the velocity distribution for a given area fraction and the mapping of the most probable velocity at different area fractions as a function of Γ. From Fig. S3A, we see that the velocity distribution profile follows a Gaussian distribution, which is consistent with such an interpretation. We also observe that the velocity increases with Γ (Fig. S3B). A systematic investigation, however, of how T_{eff} scales with Γ for different building blocks, area fractions, and shaking frequencies is beyond the scope of this paper.

Force Measurement. We measure the interaction strength and range between two pairing panels at the optimal pairing orientation on a force measurement setup composed of a single point load cell (Loadstar™) of $10^{-3}N$ resolution, USB load cell interface (DI-1000U interface, Loadstar™), a motor and a micrometer for accurate distance control (Fig. S4). We control the position of the upper panel and read out the force value from the load cell using a script written in Matlab. Starting from surface-surface contact, we separate the panels to a distance of ~ 10 cm away. As the panels approach each other, we measure the force at a set of surface-surface distances. Each force is averaged over 200 measurements to further increase the accuracy.

Dynamic Attraction Range. When placed on a flat frictional mylar surface, matching panels will spontaneously bind even when the face-to-face separation is larger than the panel thickness. To overcome friction, we gently agitate the panels vertically using a shaker table driven at an acceleration Γ (measured in units of g). We fix one panel in the center of the sample cell and place a matching panel with the right configuration and orientation at a designated distance with a pair of plastic tweezers (Fig. S5). If the attraction between panels is large enough to overcome friction forces the panels will spontaneously bind. At very high Γ the spontaneous binding is less frequent since agitation can jostle the panels into unfavorable configurations. We repeat the experiment 40-50 times, and take the distance as the attraction range when, in at least 80% of trials, the free panel immediately binds with the fixed panel.

Controlling the Polymerization of Panels. Fig. S6 shows branched polymers of three, four and five branches formed by Black, Green and Blue panels from structured seeds of three, four and five faces. Generally, we start from high acceleration and then decrease Γ to allow the polymer to grow.

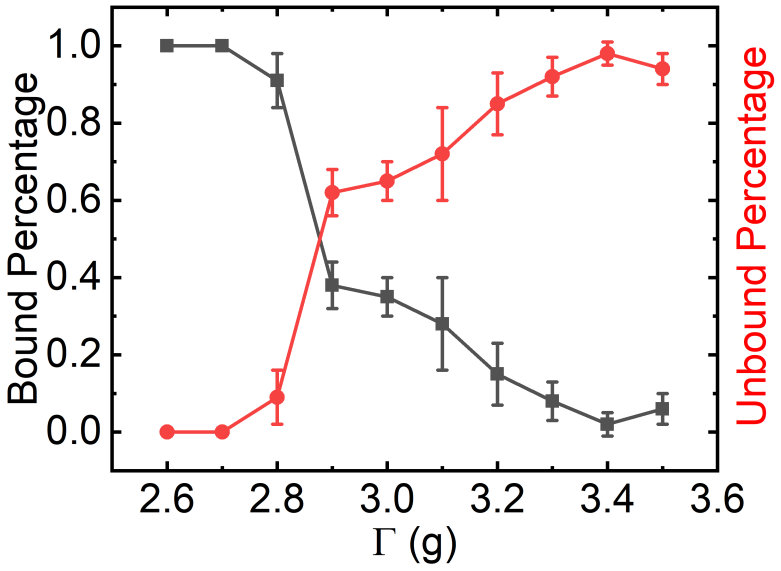

Fig. S2. Percentage of binding and unbinding of two Blue panels at different acceleration Γ.

Ran Niu[a,*], Chrisy Xiyu Du[b], Edward Esposito[a], Jakin Ng[a], Michael Brenner[b], Paul McEuen[a,c]& Itai Cohen[a,c,*]

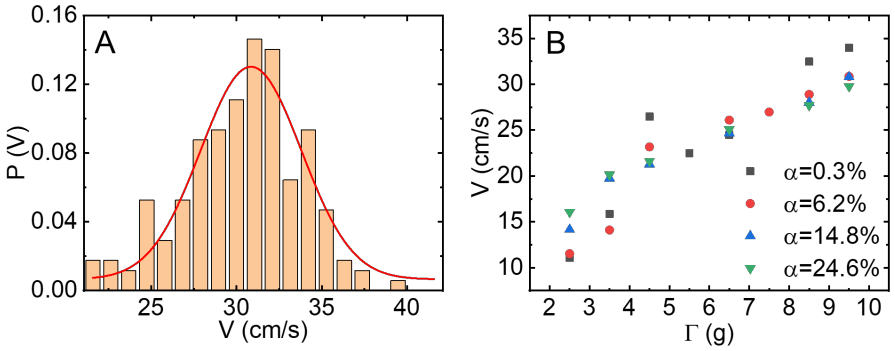

Fig. S3. Acceleration and effective temperature: A) Distribution of panel velocity at area fraction α= 6.2% and Γ=9.5g. B) Mapping of the acceleration Γ from the shaker to the mean of the panel velocity at different area fractions.

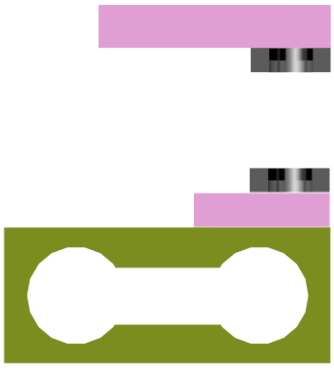

Fig. S4. Force measurement setup: We measure the magnetic interaction between two matching panels at the optimal pairing orientation on a single point load cell connected to a computer by a USB load cell interface and accurately control the surface-surface distance between panels with a motor and a micrometer mounted together.

Fig. S5. Measurement of the attraction range of panels parallel to the disk axis on a vertical vibrational shaker: We fix one panel in the center of the sample cell and place the pairing panel with the right configuration at a designated distance in a guard rail (white lines) by a pair of plastic tweezers. After released by the tweezers, the panel either directly binds to the fixed panel or jostles around. We repeat each experiment $40 - 50$ times and take the distance as the attraction range when in at least 80% of trials, the free panel is directed to bind.

Fig. S6. Branched polymer formed by Black (A), Green (B) and Blue panels (C) with three (left column), four (middle column) and five branches (right column) from structured seeds shown in the insets.

Magnetic Helix. We make helices by rotating panels on one strand relative to the matching strand. We explored how the backbone length between two panels, rotation angle of panels, panel dipole pattern and distance between pairing strands alter the pitch length. We find that panel dipole pattern has no influence on the pitch length as long as the rotation angle and the other parameters of the backbone stay the same. By decreasing the rotation angle within the range of 5-45°, we can increases the pitch length dramatically. Increasing the backbone length between two panels non-monotonically changes the pitch length. We can also add extra spacers in the back of the panels before fixing them to the strand to increase the distance of pairing strands, yielding an increase of the pitch length (Fig. 3C in the main text and Fig. S7).

Magnetic nets. For better visualization of the schematics in Fig. 4 in the main text, we show the enlarged engineering design of the 2D nets in Fig. S8.

Supplementary movies

Movie S1. Controlling the polymerization sequence of Blue/Red Janus panels (Fig. 2A iii in the main text): dimers form at $\Gamma = 3.6g$ when Blue panels bind with each other and long polymers form at $\Gamma = 2.4g$ where Red panels bind with each other. Real time speed.

Movie S2. Controlling the polymerization sequence of Green/Black, Black/Blue and Green/Blue Janus panels (Fig. 2A iv in the main text): dimers form at $\Gamma = 6.5g$, trimmers at $\Gamma = 3.9g$ and long polymers at $\Gamma = 3.0g$. Real time speed.

Movie S3. Controlling the polymerization sequence of Green/Black, Black/Blue and Green/Red Janus panels (Fig. 2A v in the main text): dimers form at $\Gamma = 6.8g$, trimmers at $\Gamma = 4.3g$ and hexamers at $\Gamma = 3.0g$. Real time speed.

Movie S4. We used structured seeds with three and four faces to form branched polymers made of Black panels. We further use a three-faced hybrid seed to grow a 3-branched hybrid polymer with two Green branches and one Black branch (Fig. 2B in the main text). Real time speed.

Movie S5. We use magnetic strands to create secondary structures, including S-shaped curves, hairpins and helices. We can also do the toehold exchange with magnetic strands (Fig. 3B-D in the main text). Real time speed.

Movie S6. Hierarchical self-assembly of 2D nets into 3D structures (Fig. 4 in the main text). Real time speed.

Movie S7. When we do not include the information of panel dipole pattern and orientation into the design of 2D nets, the 2D nets fall into metastable configurations under vibration. Real time speed.

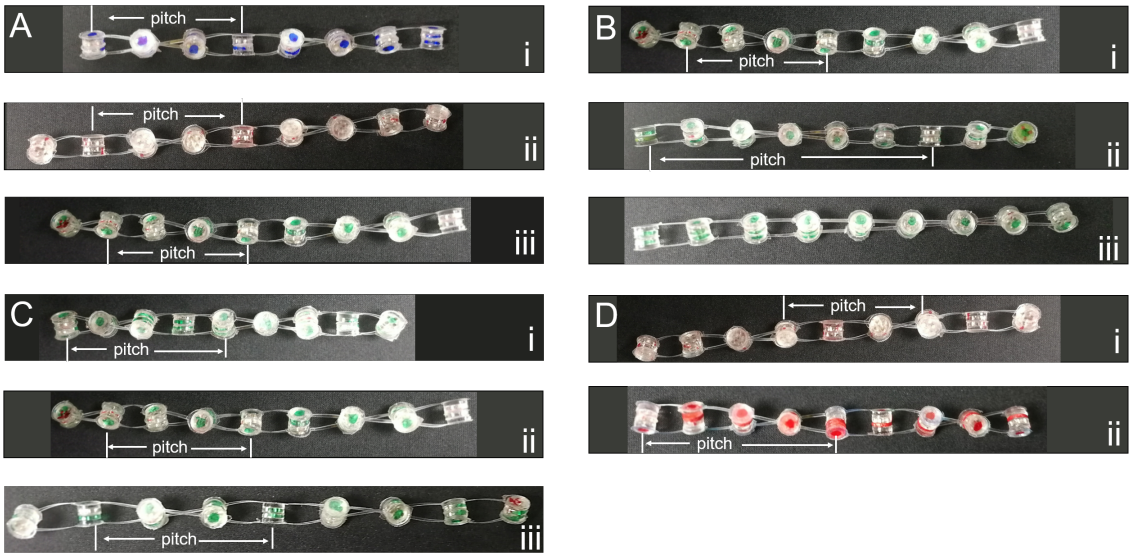

Fig. S7. Magnetic helices: A) We make helices from (i) Blue, (ii) Red and (iii) Green panels and elastic materials by rotating panels on one strand with 45° relative to the pairing strand. The pitch length is the same for the three helices. B) By rotating green panels on one strand with (i) 45°, (ii) 25°, and (iii) 15°, we increase the helical pitch from 7.0 cm to 13.1 cm to larger than 17.2 cm. C) By keeping the rotation angle fixed and increasing the backbone length between green panels from (i) 0.76 cm to (ii) 1.14 cm to (iii) 1.52 cm, We find a slight non-monotonic change of the helical pitch as both the number of panels in one pitch and the distance between nearby panels change. D) By adding an additional spacer in the back of each panel before fixing them onto the strand and keep the other parameters unchanged, we increase the distance of pairing strands, yielding an increase of the pitch length from (i) 7.0 cm to (ii) 9.1 cm.

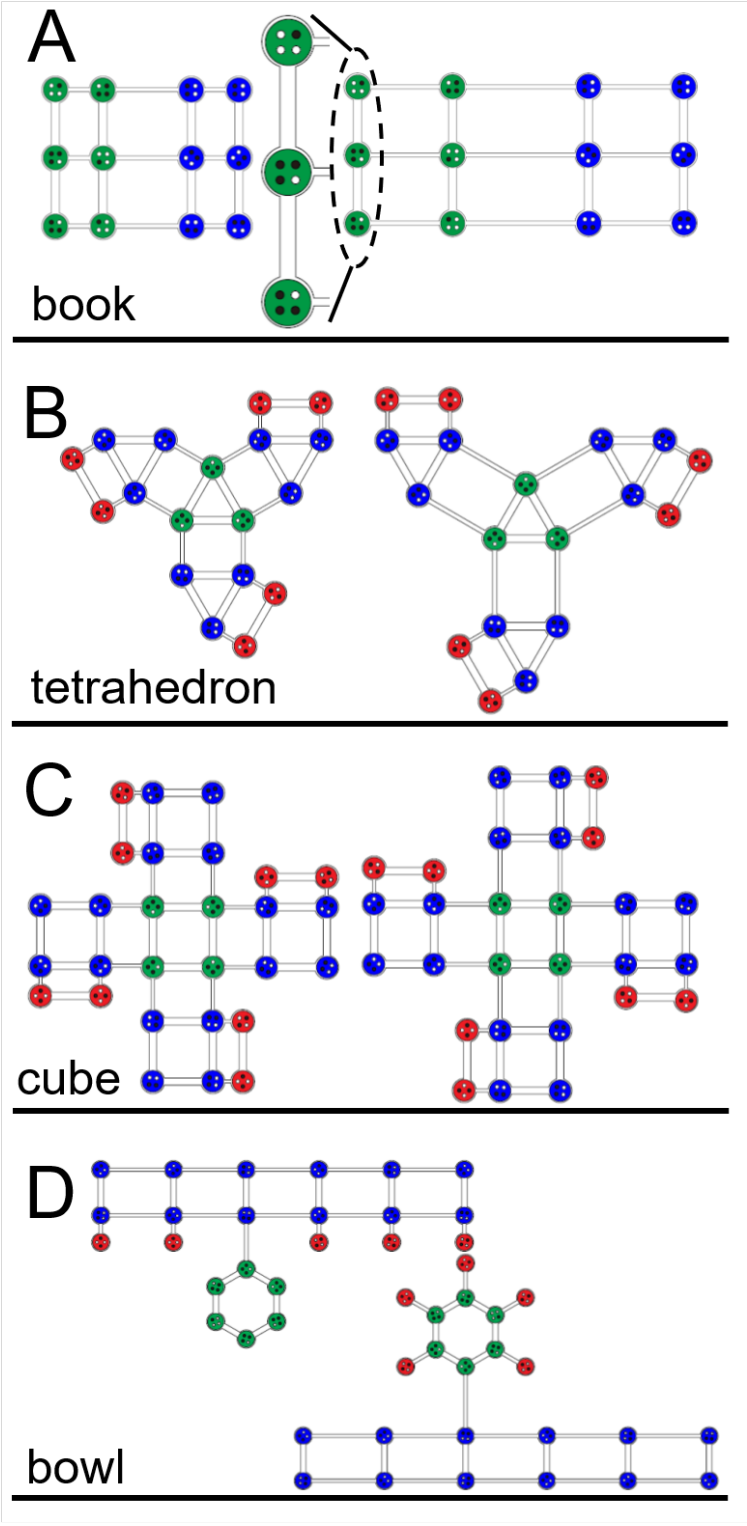

Fig. S8. Hierarchical self-assembly of 2D nets into 3D structures. Engineering design of 2D nets used to assemble into (A) a book; (B) a tetrahedron; (C) a cube; and (D) a bowl.